Research Paper

3D-printed PLA/PCL Scaffolds for Glenohumeral Joint Repair: Effect of Pore Architecture and Composition

Hosein Rostamani[1], Omid Fakhraei[2*], Melina Jalalian[2], Amirmohammad Shabanzadeh[2], Fatemeh Rahdari[2], Minoo Fanaei Bonakdar[2]

1. Department of Biomedical Engineering, School of Biomedical Engineering, Amirkabir University of Technology (Tehran Polytechnic), Tehran, Iran.
2. Department of Biomedical Engineering, Ma.C., Islamic Azad University, Mashhad, Iran.

Use your device to scan and read the article online

Citation Rostamani H, Fakhraei O, Jalalian M, Shabanzadeh A, Rahdari F, Fanaei Bonakdar M. 3D-printed PLA/PCL Scaffolds for Glenohumeral Joint Repair: Effect of Pore Architecture and Composition. Journal of Translational Regenerative Medicine. 2026; 1:E1026. http://dx.doi.org/10.32598/JTRM.1.1026

http://dx.doi.org/10.32598/JTRM.1.1026

ABSTRACT

Background: Cartilage tissue-engineering scaffold design has mostly focused on the knee joint, leaving the mechanically distinct glenohumeral joint comparatively understudied. This joint is muscle-loaded across a wide, multidirectional arc rather than along one fixed axis, and its cartilage is thin, favoring an osteochondral rather than purely chondral scaffold format. This study aimed to identify a scaffold configuration suited to the mechanical and geometric limitations of the glenohumeral joint by using three-dimensional (3D)-printed polylactic acid (PLA) and polycaprolactone (PCL) scaffolds with varying pore architecture and composition.

Methods: In this study, porous PLA and PCL scaffolds varying in pore architecture (honeycomb, gyroid) and composition (PLA, PCL, layered hybrid PLA-PCL) were 3D printed and assessed by Fourier-transform infrared (FTIR) spectroscopy, water contact angle (WCA) measurement, optical microscopy, and mechanical testing (uniaxial compression, three-point bending).

Results: Gyroid architecture reduced elastic modulus to 34–49% compared to the honeycomb architecture across all compositions, moving bulk stiffness closer to native cartilage, and behaved near-isotropically, whereas honeycomb architecture lost most of its stiffness and strength when loaded off-axis. The specimens with gyroid architecture also failed gradually under bending rather than fracturing suddenly. PLA was stiffer and stronger than PCL and the hybrid scaffolds in both architectures. PCL and the hybrid traded elastic modulus against plateau strength. FTIR spectroscopy showed no chemical alteration from printing, and apparent WCAs matched values for flat PLA and PCL films reported in the literature, except for a lower-than-expected WCA for PCL, attributed to surface roughness.

Conclusion: Given its stiffness, near-isotropic behavior, non-brittle failure, and more tunable degradation than PCL alone, a layered PLA-PCL scaffold with gyroid architecture is recommended for further glenohumeral joint application studies.

Keywords: Polylactic acid (PLA), Polycaprolactone (PCL), Three-dimensional (3D) printing, Osteochondral, Biomaterials

Article info:
Received: 10 Oct 2025
Accepted: 15 Dec 2025
Publish: 14 Jan 2026

*** Corresponding Author:**
Omid Fakhraei, Assistant Professor.
***Address:** Department of Biomedical Engineering, Ma.C., Islamic Azad University, Mashhad, Iran.*
***Phone:** +98 (936) 1351735*
***E-mail:** omid.fakhraei@iau.ac.ir*

Highlights

- This study targeted scaffold design for the understudied, multidirectional glenohumeral joint.
- Scaffolds with gyroid architecture had a lower elastic modulus by 34–49% than those with honeycomb architecture.
- Off-axis honeycomb specimens lost most stiffness, while gyroid specimens stayed isotropic.
- Gyroid scaffolds bent gradually, while honeycomb fractured suddenly.
- A layered PLA-PCL scaffold with gyroid architecture is recommended for glenohumeral joint repair.

Plain Language Summary

Cartilage is the smooth tissue that covers the ends of bones in a joint and helps them move with little friction. When severely damaged, cartilage has limited ability to repair itself. One approach under investigation uses a scaffold, a temporary structure designed to support the growth of new tissue. Most research on cartilage scaffolds has focused on the knee, although joints such as the shoulder experience different patterns of movement and loading. In this study, we investigated three-dimensional (3D)-printed scaffolds made from two biodegradable polymers, polylactic acid (PLA) and polycaprolactone (PCL). We compared two internal structures: a honeycomb-like design and a continuous, three-dimensional design called a gyroid. We tested each material alone and in a layered combination. We then examined the scaffolds' chemical and surface properties and assessed how they responded to different types of loading. The gyroid design showed several mechanical properties that may be useful for a shoulder scaffold. It was less stiff under compression, bringing its behavior closer to that of natural cartilage. Its mechanical performance also varied less when loads were applied from different directions, and it deformed and failed more gradually rather than breaking suddenly. Among the materials tested, the layered PLA/PCL scaffold offered a promising balance of mechanical properties and the potential to adjust how it degrades over time. These findings may help guide the development of cartilage-repair scaffolds designed for the shoulder. However, the results are preliminary. The scaffolds were tested without living cells or the fluid-rich environment of natural cartilage. Studies incorporating biological materials and evaluating long-term mechanical and biological performance are needed before clinical use can be considered.

Introduction

Articular cartilage is avascular, aneural, and alymphatic, leaving it with almost no capacity for spontaneous repair. Focal defects that go untreated tend to progress towards osteoarthritis rather than heal, and current treatments, including microfracture, osteochondral autografts and allografts, and autologous chondrocyte implantation, remain limited due to fibrocartilage formation, donor-site morbidity, or multi-stage procedures [1, 2]. Tissue-engineered scaffolds that provide a mechanically appropriate, permissive environment for chondrocytes are an alternative to these approaches. Scaffold design increasingly depends on matching architecture and composition to the specific joint being treated rather than treating cartilage as a single generic target.

Most scaffold design efforts have targeted the knee. The glenohumeral joint is comparatively understudied despite presenting a genuinely different problem. Focal chondral defects in this joint are less common than in the knee and usually surface incidentally during arthroscopy for instability, rotator cuff pathology or trauma, and management options remain limited [3]. Mechanically, the joint is muscle-loaded rather than weight-bearing, but the loads involved are not trivial: in vivo telemetry from instrumented shoulder implants records contact forces below 100% body weight (BW) for most activities of daily living, rising to around 130% BW near the limits of motion, with peaks of up to 238% BW during forward flexion and abduction [4-6]. The shallow glenoid also produces a small contact patch that migrates across the humeral head through a wide arc of motion; therefore, there is no single fixed loading axis to design around, and shear and sliding are prominent alongside compression. A scaffold for the glenohumeral joint should tolerate load from many directions rather than resist load along one. Another limitation is geometric. Humeral head cartilage is thin (1.4-1.8 mm) [7], and this limits what a porous architecture can achieve at that thickness. At practical layer heights and unit-cell sizes, a purely chondral-depth construct can contain too few unit cells through its thickness to behave as the intended lattice rather than an arbitrary perforated solid, since Gibson-Ashby scaling requires 5-10 unit cells through the loaded dimension for the architecture's bulk properties to hold [8]. This favors an osteochondral rather than a purely chondral scaffold format, in which a several-millimeter-deep construct leaves room for a genuine lattice, with a deeper phase carrying the mechanical load and a superficial phase serving as the chondral compartment.

Three-dimensional (3D) printing (material extrusion) is used to fabricate the scaffolds because it allows pore architecture and composition to be specified and reproduced directly, to a degree that conventional fabrication routes cannot match, and graded. Site-specific scaffold designs of this kind have increasingly been explored for osteochondral repair [9-11]. The first study design variable is composition. Polylactic acid (PLA) and polycaprolactone (PCL) both are biodegradable, biocompatible aliphatic polyesters already used in tissue engineering, but they behave very differently over time. PLA is comparatively stiff and loses mechanical strength relatively early, well before its own multi-year degradation window closes, while PCL is far more compliant and persists mechanically for upwards of two years in vivo, with fragmentation only beginning around thirty months [12-15]. This mismatch has motivated testing a layered PLA/PCL hybrid, PCL-rich towards the articulating surface, and PLA-rich in the deep phase, alongside the two single-polymer groups. The second design variable is pore geometry, a conventional strut-based honeycomb against a gyroid, a triply periodic minimal surface whose triple connectivity has been reported to give more isotropic mechanical behavior and more uniform permeability than strut-based lattices [16], properties that are important for a joint without a fixed loading axis and for a tissue that depends entirely on diffusion for nutrient supply. Because chondrocyte phenotype is sensitive to cell shape, with flattened, spread morphologies favoring a shift from type II towards type I collagen expression [17, 18], the continuously curved pore walls of a gyroid may also offer a more favorable surface for maintaining a rounded, differentiated phenotype than the flat faces of a honeycomb.

In this study, porous PLA/PCL scaffolds varying in pore architecture (honeycomb, gyroid) and composition (PLA, PCL, and a layered PLA/PCL hybrid) were designed, printed, and characterized by suing the Fourier-transform infrared Fourier-transform infrared spectroscopy (FTIR) spectroscopy, water contact angle (WCA), optical microscopy, and mechanical testing under uniaxial compression and three-point bending, for identifying a scaffold configuration suited to the mechanical and geometric constraints of the glenohumeral joint ahead of subsequent hydrogel integration and biological evaluation.

Materials and Methods

Scaffold design

PLA and PCL filaments, 1.75 mm in diameter (±0.05 mm), were used in this study. Two porous unit-cell architectures were designed for each material composition: a honeycomb lattice (directionally ordered, prismatic pores) and a gyroid lattice (a triply periodic minimal surface with near-isotropic, fully interconnected pores). During preliminary design, matching porosity alone between the two architectures was judged insufficient, since equivalent porosity can be produced either by a few large pores or by many small ones; therefore, pore size was matched explicitly as an independent design variable. The final scaffold geometry used for all reported testing had an overall footprint of 20×20×5 mm, a nominal pore size ≈ 300 µm, target porosity of 50%, and a design layer thickness of 0.1 mm.

Three material compositions were produced for each architecture: Pure PLA, pure PCL, and a layered PLA/PCL hybrid. The hybrid group was built as a three-layer laminate (PLA–PCL–PLA), with the total layer count matched to that of the corresponding single-material scaffolds and PCL confined to the fully embedded middle layer. This configuration was adopted after pilot builds showed that whichever layer ended up outward-facing after printing was prone to poor interlaminar bonding when it was PCL; a four-layer build in particular always leaves a PCL layer exposed at the top, which delaminated. Builds with PLA placed in the middle layer also failed to bond and were reported as a negative finding rather than as the adopted protocol.

Fabrication by fused deposition modeling

Scaffolds were fabricated by a fused deposition modeling (FDM) printer, PLA was processed within 180–220 ˚C and PCL within 80–120 ˚C, narrowing to approximately 200–210 ˚C for PLA and 90–130 ˚C for PCL; nozzle diameter was 0.2–0.4 mm, bed temperature 30–60 ˚C, print speed 20–60 mm/s, and ambient (room) temperature was maintained at approximately 23–25 ˚C. A

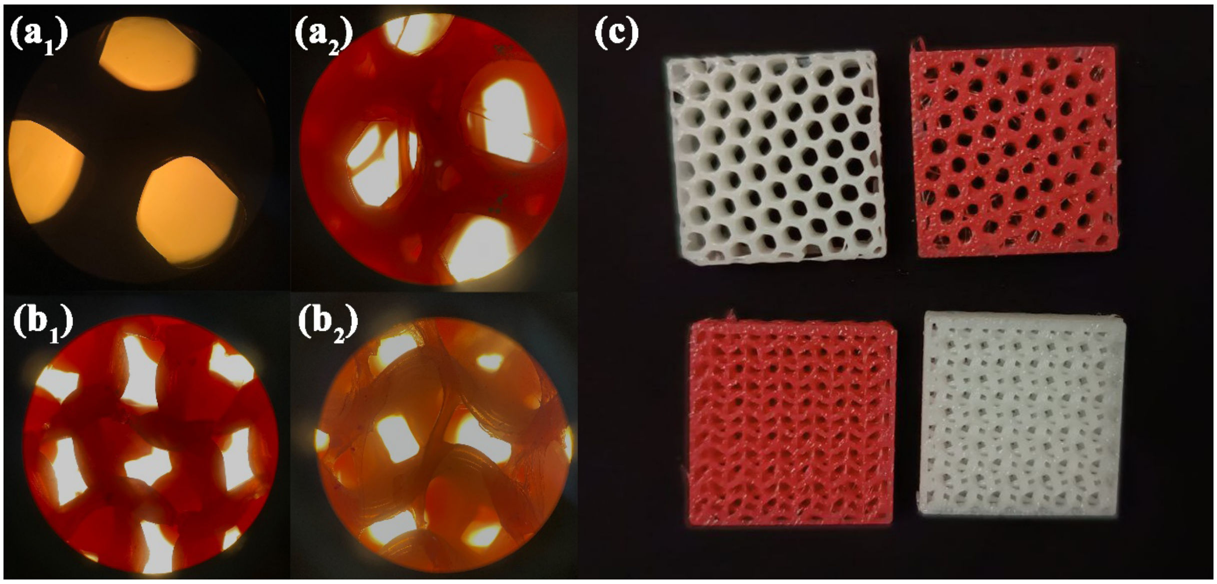

Figure 1. Optical microscopy images of (a) gyroid scaffolds and (b) honeycomb scaffolds; (c) Macroscopic (naked-eye) images of a number of the printed scaffolds

preliminary print trial compared two nominal infill/print densities (30% and 60%) for both architectures. The PLA/PCL hybrid group was printed on a single-nozzle printer, with the two materials deposited in sequence rather than a dedicated dual-extrusion setup.

Surface wettability

Surface wettability was assessed in the PLA and PCL groups using an apparatus from APEX Technologies Co., Iran (Model IFT-PDSA-02). Measurements were taken from the lateral surface of each specimen rather than the top or base face, since the pores intersecting the flat top/base surfaces were judged likely to bias the measurement, whereas the side surface was less affected. A droplet of deionized water (2–3 µL) was placed on the surface and imaged by a laboratory goniometer; the apparent WCA was extracted from the droplet profile, with a 1 mm scale bar included in each image. Automated fits that failed on the rough, porous surface were visually screened and excluded. As an independent check, WCA was also calculated geometrically from droplet width and height measured against the same scale bar. As the droplet footprint spanned roughly three pores, re-

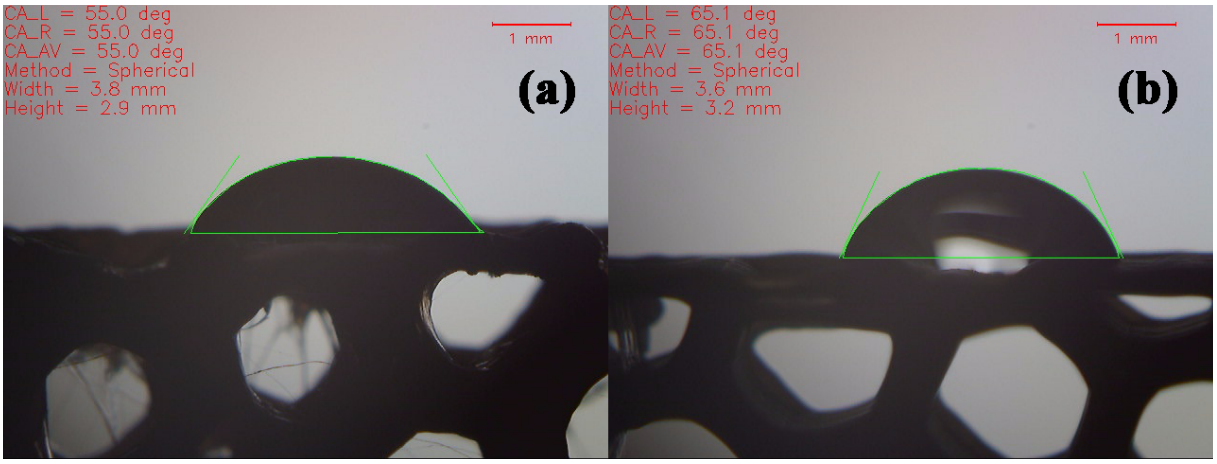

Figure 2. The WCA measurements on the honeycomb scaffold surface

a) PCL, b) PLA

Note: The green color shows the fitted droplet profile (spherical method); scale bar=1 mm.

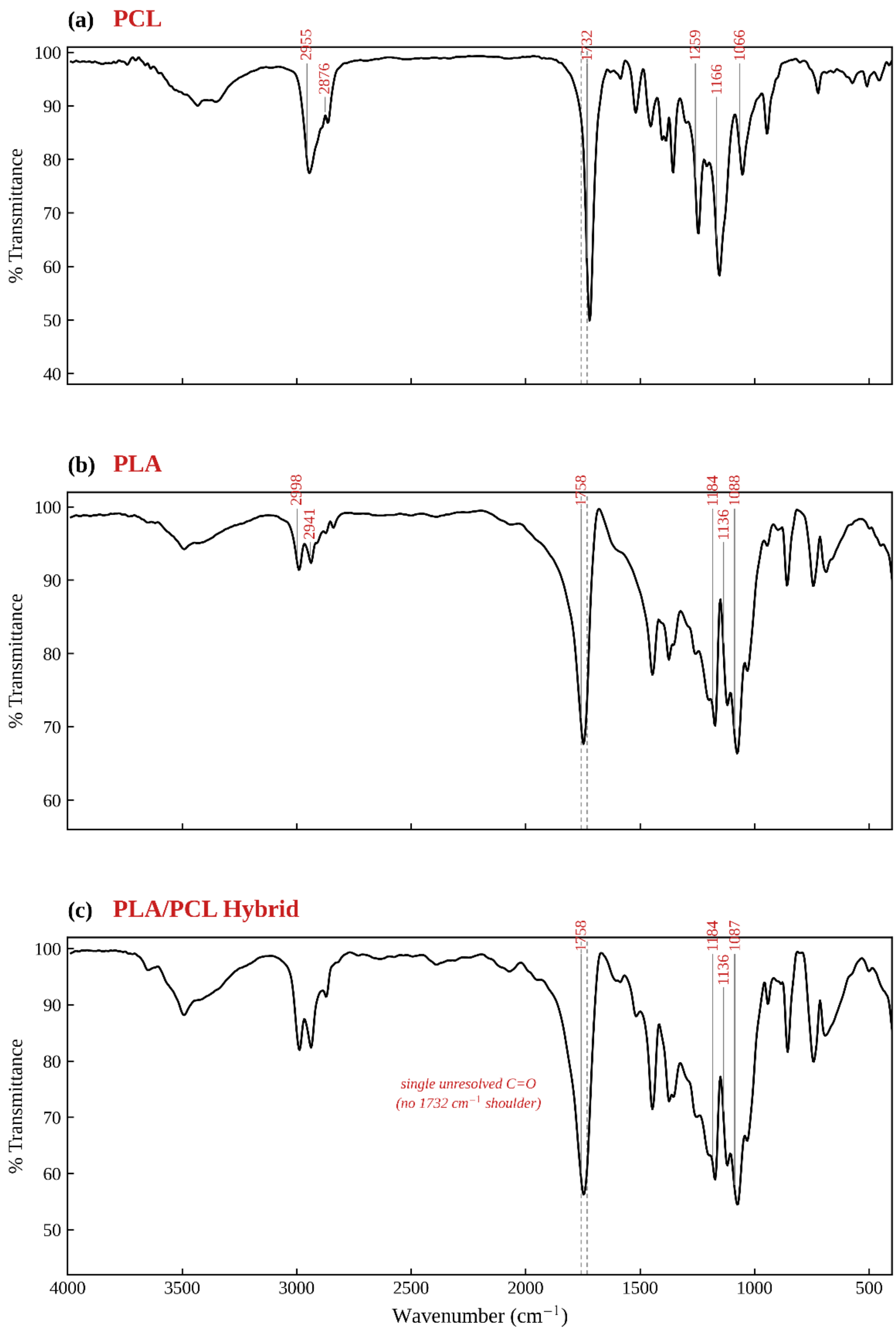

Figure 3. FTIR spectra of (a) PCL, (b) PLA, and (c) PLA/PCL hybrid scaffolds

Note: Labeled bands correspond to the characteristic functional-group absorptions; dashed lines mark the PCL (1732 cm^{-1}) and PLA (1758 cm^{-1}) carbonyl stretching positions for comparison across panels. The hybrid scaffold's spectrum closely matches the PLA's in both carbonyl position and fingerprint region, with no separately resolved PCL carbonyl shoulder.

Table 1. Apparent WCA of honeycomb specimens (n=5)

Group	Mean Apparent WCA	Range Across Fitting Methods	Geometric Check Angle
PCL / honeycomb	≈56°	54.9–58.9°	57°
PLA / honeycomb	≈66.7°	63.5–71.8°	65.2°

ported values represent an apparent (composite-surface) contact angle rather than the intrinsic wettability of the bulk polymer.

Fourier-transform infrared spectroscopy

FTIR spectroscopy (Nicolet is10, Thermo Fisher Scientific) was performed on three specimens: one with a pure PLA scaffold, one with a pure PCL scaffold, and one with a PLA/PCL hybrid scaffold. The spectra were obtained over a scanning range of 400–4000 cm^{-1} with a resolution of 4 cm^{-1} at room temperature. This test was used to confirm that the printed scaffolds retained the expected polymer functional groups and were not chemically altered by the printing process.

Optical microscopy

Printed strand morphology and pore geometry were examined by optical microscopy to verify fidelity of the printed lattice to the design and to document realized pore/strut dimensions. Immediately after printing, scaffolds (3 per group) were imaged with a stereomicroscope at low magnification (to capture the overall lattice) and at high magnification (to resolve individual strand and pore boundaries), across three non-overlapping fields per scaffold.

Mechanical testing

Uniaxial compression

Compression testing was in accordance with the ASTM D695-15 standard. Specimens were loaded to failure or to a protocol limit, reached at widely differing nominal strains across groups (20–98%); therefore, peak force was not compared directly across groups, and inter-group comparisons were instead made at fixed strain (10% and 20%). Elastic modulus (E) was considered as the steepest tangent to the stress–strain curve within the initial pre-yield region. Strain energy density absorbed to 20% strain (U@20%) was calculated as the area under the stress–strain curve up to that strain.

Three-point bending

Flexural testing was in accordance with a three-point bending configuration (ASTM D790-17 standard), with applied load perpendicular to the scaffold surface. Crosshead speed was set according to specimen thickness: 1 mm/min for 3 mm-thick specimens and 2 mm/min for 5 mm-thick specimens. For the layered hybrid group, specimens were loaded transversely (cross-sectional) rather than the outward-facing single-material surface, so that the recorded response reflects the combined bilayer material system rather than only the outermost material. Flexural modulus was taken as the initial tangent slope of the load–deflection curve and flexural peak stress as the maximum recorded stress. Since several specimens (particularly gyroid and PCL-containing groups) did not fracture and continued to carry load well beyond 10% flexural strain, values beyond this point

Table 2. FTIR band assignments (cm^{-1})

Assignment	PCL Specimen	PLA Specimen	Hybrid Specimen
C–H stretching	2955, 2876	2998, 2941	2997, 2950, 2880
C=O ester stretch	1732	1758	1758
CH_2/CH_3 bending	1470, 1401, 1369	1458, 1386	1458, 1386, 1364
C–O–C stretching	1259, 1166, 1066	1184, 1136, 1088	1184, 1136, 1087
Skeletal / rocking	735	873, 757, 700	869, 756, 707

Table 3. Compression test results

Group	Mean±SD				CV of E
	E (MPa)	σ@10% (MPa)	σ@20% (MPa)	U@20% (MJ/m^3)	
PLA/honeycomb (n=3)	381±13	17.2±1.1	22.4±1.4	3.22	3%
PLA/gyroid (n=3)	130±14	6.2±0.6	6.5±0.6	1.08	11%
PCL/honeycomb (n=3)	43.7±4.6	3.08±0.31	3.7±0.38	0.54	10%
PCL/gyroid (n=3)	16.4±0.8	1.07±0.07	1.21±0.06	0.18	5%
PLA-PCL/honeycomb (n=2)	30.7±15.5	2.2±0.3	4.7±0.2	0.47	50%
PLA-PCL/gyroid (n=3)	15.1±7.3	1.2±0.2	2.3±0.3	0.25	48%

Abbreviations: E: Elastic modulus; σ : Stress; U: Strain energy density; CV: Coefficient of variation.

exceeded the small-deflection assumptions of standard beam theory and were reported as apparent/indicative flexural properties.

Results

Optical micrographs (Figure 1) confirmed that both architectures printed with pore geometry matched their respective designs. Gyroid specimens (Figure 1a) showed open, well-interconnected pores with smoothly curved, rounded boundaries and no sharp internal corners, consistent with the triply periodic minimal surface design. Pore openings were of broadly similar size within a given field, and the strut/wall surfaces showed a continuous, slightly textured finish. Honeycomb specimens (Figure 1b) showed a visually distinct geometry; two sets of printed strands crossing at an angle were clearly resolvable, bounding pore openings with straighter, more angular edges than the gyroid, consistent with the directionally-ordered, raster-based construction of this architecture, and individual deposition lines were visible along the strand surfaces.

The WCA was measured on the lateral surface of PLA and PCL honeycomb specimens (Table 1). For PCL, four of five automated fitting methods gave a mean apparent WCA of approximately 56° (ranged 54.9–58.9°). The fifth method returned a 42° left–right discrepancy (49.6° vs 91.6°) and was excluded as an invalid fit. An independent geometric calculation from droplet width and height gave a consistent value of approximately 57° (Figure 2). For PLA, the five fitting methods agreed more closely, giving a mean apparent WCA of approximately 66.7° (ranged 63.5–71.8°), with the geometric

Table 4. Bending test results

Group	Mean±SD		CV of E_{flex}
	E_{flex} (MPa)	σ_{peak} (MPa)	
PLA/honeycomb (n=3)	139±10	19±2	7%
PLA/gyroid (n=3)	71.6±3.6	11.7±0.8	5%
PCL/honeycomb (n=3)	8.7±4.3	3±1.3	49%
PCL/gyroid (n=3)	8.7±2.5	2.1±0.7	29%
PLA-PCL/honeycomb (n=3)	29.3±2.2	6.2±0.8	8%
PLA-PCL/gyroid (n=3)	13.5±6.4	3±1	47%

Abbreviations: $E_{flex:}$ Flexural modulus; σ_{peak}: Peak stress; CV: Coefficient of variation.

Note: Values beyond 10% flexural strain were apparent/indicative.

check giving 65.2°. As the droplet footprint spanned several pores of the ~300 µm design pore size, these values represent an apparent, composite-surface contact angle rather than the intrinsic wettability of the bulk polymer.

FTIR spectra of the PLA, PCL, and PLA/PCL hybrid scaffolds (Figure 3) showed absorption bands consistent with each polymer's expected functional groups, with no additional bands indicating chemical alteration during printing (Table 2). The PCL scaffold showed its characteristic ester C=O stretch at 1732 cm^{-1}, CH_2 stretching at 2955 and 2876 cm^{-1}, and C–O–C stretching bands at 1259, 1166, and 1066 cm^{-1}. The PLA scaffold showed the carbonyl stretch at a higher wavenumber (1758 cm^{-1}), together with CH_3 stretching at 2998 and 2941 cm^{-1} and a C–O–C fingerprint triplet at 1184, 1136, and 1088 cm^{-1}. The hybrid scaffold's spectrum closely matched the pure PLA spectrum in both the carbonyl position (1758 cm^{-1}) and the fingerprint region (1184, 1136, 1087 cm^{1}); a separately resolved PCL carbonyl feature near 1732 cm^{-1} was not apparent. This is consistent with the laminate design, in which PLA forms both outward-facing layers and PCL is confined to the embedded middle layer. Therefore, a specimen-surface FTIR measurement predominantly samples PLA.

Regarding mechanical behaviors, specimens reached widely differing final strains before the protocol limit or failure (20–98% nominal). Therefore, peak force was not compared across groups. Comparisons presented in Table 3 were made at a fixed strain.

At matched composition, gyroid reduced elastic modulus to 34–49% of the corresponding honeycomb value (PLA: 130 vs 381 MPa; PCL: 16.4 vs 43.7 MPa; hybrid: 15.1 vs 30.7 MPa). PLA scaffolds were considerably stiffer and stronger than either PCL or the hybrid scaffolds, in both architectures. Between two candidate chondral-phase compositions, PCL scaffolds had the higher elastic modulus in both architectures (43.7 vs 30.7 MPa for honeycomb; 16.4 vs 15.1 MPa for gyroid), while the hybrid scaffolds had the highest stress at 20% strain in both architectures (4.7 vs 3.7 MPa for honeycomb; 2.3 vs 1.21 MPa for gyroid).

A single PLA/honeycomb specimen tested with the load axis rotated 90° from the standard build orientation gave E = 38.6 MPa and σ@20% = 2.73 MPa, approximately 10-fold and 8-fold lower, respectively, than the same group tested conventionally (381 MPa and 22.4 MPa).

Gyroid again reduced flexural modulus more compared to the matched honeycomb for PLA (71.6 vs 139 MPa; 52%) and the hybrid (13.5 vs 29.3 MPa; 46%), but not for PCL, where flexural modulus was similar between the two architectures (8.7±2.5 vs 8.7±4.3 MPa). In terms of composition, PLA scaffolds ranked first, followed by hybrid and PCL scaffolds, for both flexural modulus and peak stress, consistently across both architectures (Table 4).

The PLA specimen with honeycomb architecture lost load abruptly in two of three replicates, while all three types of specimens with gyroid architecture declined gradually and continued to carry load past 55% flexural strain without a discrete fracture event; several PCL-containing specimens and those with gyroid architecture did not fracture within the tested range at all.

Discussion

In all three scaffold compositions, those with gyroid architecture had a lower elastic modulus (by 34–49%) compared to those with honeycomb architecture. The PLA specimen with honeycomb architecture that was loaded 90° from the standard build orientation was roughly 10-fold less stiff and 8-fold weaker than the same specimen loaded conventionally. Both observations have the same structural cause. A honeycomb is a strut-based, prismatic lattice; the load applied along the strut axis is carried in tension/compression, a stretching-dominated, mechanically efficient mode that gives high stiffness, while load applied off-axis is carried by strut bending, which is far more compliant. A gyroid is a shell-based triply periodic minimal surface with continuous curvature and connectivity in all three principal directions; it has no aligned strut to carry load efficiently along any one axis; thus, its behavior is bending-dominated throughout, consistent with mechanical characterization of triply periodic minimal surface scaffolds [16], which makes it softer on average and close to isotropic. Pore geometry has similarly been shown to substantially modulate mechanical response in FDM-printed single-polymer PCL scaffolds [11].

The gyroid architecture moderates stiffness with no built-in weak axis, and suits the glenohumeral joint better than the honeycomb architecture. This joint has no fixed principal loading axis; therefore, a lattice with a weak direction risks failure whenever the small, migrating glenoid contact patch loads it off-axis. For human knee articular cartilage, a study reported an equilibrium modulus of 7.48±4.42 MPa, a Young's modulus of 1.03±0.48 MPa, a dynamic modulus of 7.71±4.62 MPa at 1 Hz, and an instantaneous modulus of 52.14±9.47 MPa at 1 mm/s [19]. The PLA specimen with honeycomb architecture, at 381 MPa, overshoots this envelope by roughly an order of magnitude regardless of loading rate. The PLA specimen with gyroid architecture, at 130 MPa, remained stiff compared to native tissue but sits far closer to the instantaneous end of the range. The PCL and hybrid specimens with gyroid architecture (15–16 MPa) sit closer still. Architecture is, therefore, an effective factor for bringing bulk stiffness toward the normal range, leaving composition free to be chosen mainly on degradation and surface-chemistry grounds. The gyroid's continuous, concave pore-wall curvature may also favor chondrocyte phenotype maintenance more than the honeycomb's flat faces. Chondrocyte dedifferentiation, the shift from type II toward type I collagen expression, is directly linked to cell shape; dedifferentiated cells re-express the differentiated phenotype once returned to a rounded, anchorage-independent geometry [17], and dedifferentiation probability increases with increasing area and aspect ratio at the single-cell level [18]. A concave surface limits spreading more than a flat surface, consistent with better retention of the rounded morphology associated with the differentiated state.

Regarding bending, the gyroid architecture's effect showed up as a failure mode. The PLA specimen with honeycomb architecture lost load suddenly in two of three replicates, whereas all three types of specimens with gyroid architecture declined gradually and continued carrying load past 55% flexural strain without a discrete fracture event. Brittle, sudden failure in a joint generates particulate debris and a synovitis risk, avoiding gradual yielding.

The PLA scaffold was stiffest and strongest regardless of its architecture, but between the two PLA and PCL scaffolds, PCL had the higher elastic modulus in both architectures, while the hybrid PLA-PCL scaffold had the highest stress at 20% strain in both architectures. Since both metrics describe resistance to progressive collapse as the structure is compressed further, and that plateau behavior is what matters under sustained joint load, the mechanical case for the hybrid PLA-PCL scaffold compared to the PCL scaffold is not clear, but it is not unfavorable either.

Regarding degradation, PCL is exceptionally persistent. Capsules with an initial Mw ≈ 66,000 g/mol have been reported to remain intact in shape through two years of implantation, only fragmenting into low-molecular-weight pieces at around 30 months [12], well past the point at which a chondral-phase scaffold should have resorbed and been replaced by neotissue. PLA offers a way to tune this, since poly-L-lactide (PLLA) loses mechanical strength within one-fifth of its own 3–5 year full-degradation window, an approach already applied to PLA/PCL blends in other osteochondral contexts [10]. This aligns with the reported degradation behavior of each polymer individually rather than a direct measurement on the printed laminate, and would need confirmation with a degradation study on the actual scaffold. Non-mechanical considerations also support the favorability of the hybrid scaffold. Thermoformability, relevant to conforming a thin construct to the convex humeral head surface (coronal radius of curvature ≈ 24 mm [20]), and its already-stratified structure, which maps onto both the zonal organization of native cartilage and the osteochondral transition that graded, site-specific scaffold designs of this kind are intended to reproduce [9–11].

Building the hybrid scaffold as a laminate rather than a blend has direct consequences visible in the outcome. Interlaminar bonding is a plausible source of the variability seen in the hybrid scaffolds, which showed the greatest coefficients of variation for both elastic modules (48% and 50% for honeycomb and gyroid) and flexural modules (8% and 47% for honeycomb and gyroid). PLA is deposited at 200–210 °C and PCL at 90–130 °C; therefore, the PLA-on-PCL interface places molten polymer onto a substrate far below its own processing temperature, and the PCL-on-PLA interface deposits too cool to reheat and weld the layer beneath it. Bond strength at each interface thus depends on local thermal history, which is expected to vary across a part and between builds, consistent with the scatter observed. This also supports the pilot-stage finding that an outward-facing PCL layer delaminated and that placing PLA in the middle layer of a four-layer build failed to bond: both indicate interlayer adhesion, not either bulk material, as the weak link in this fabrication route. Part of this difference may also be due to the hybrid scaffold being printed by sequential single-nozzle deposition rather than true dual-extrusion, a fabrication method different from any intrinsic PLA–PCL bonding. Furthermore, degradation in a laminate is expected to be layer-selective rather than uniform. PLA hydrolyses faster than PCL, and the process is autocatalytic, since cleaved ester bonds generate acid end groups that accelerate further hydrolysis [12]. In a blended material, these products would disperse, while in a laminate they are expected to concentrate in discrete planes, producing local pH drops those chondrocytes tolerate poorly, with preferential loss of the PLA layers eventually leaving a delaminating PCL stack. This is a smaller concern in the glenohumeral joint than in most tissues, because the glenohumeral joint's substantial synovial fluid volume and turnover, together with the scaffold's interconnected porosity, both favor rapid clearance of degradation products rather than local accumulation.

The glenohumeral joint's mechanical demands help calibrate how much stiffness reduction is actually useful. Bergmann et al., in an in vivo telemetry study of instrumented shoulder implants, showed contact forces below 100% BW for most activities of daily living, reaching about 130% BW close to the limits of motion or against external resistance [4]. In another study, they showed that lifting up a 1.5 kg object with a straight arm led to an average force of 105% BW, while setting the object down led to an average force of 123% BW [5]. In another study, they reported peak forces up to 238% BW during forward flexion and abduction of the arm [6]. These are moderate loads relative to the lower limb, and the PLA scaffold with honeycomb architecture at 381 MPa was correspondingly over-engineered for this joint.

A study on humeral head cartilage reported a central thickness of 1.77±0.35 mm, and the superior and inferior thicknesses were both 1.42 mm. For the glenoid cavity, it had a reciprocal pattern; cartilage was thickest superiorly and inferiorly (2.61±0.47 mm and 2.53±0.58 mm) and thinnest centrally (1.69±0.22 mm) [7]. The 5 mm-thick scaffold specimens characterized in our study therefore do not directly represent a construct built at native chondral thickness. At the layer heights used, 1.5 mm thickness corresponds to only 5-7 printed layers, and if the gyroid unit cell was 1–2 mm, less than one full period would exist with that thickness, when the lattice no longer behave as the intended periodic architecture: both Gibson-Ashby scaling and the isotropy argument require on 5-10 unit cells through the loaded dimension for the architecture's bulk properties to hold [8]. This is the underlying reason for testing and eventually building an osteochondral rather than a purely chondral construct, consistent with the graded, site-specific designs increasingly explored for osteochondral repair [9–11]. A several-millimeter deep plug leaves room for a genuine lattice, with the deep phase carrying the mechanics and the superficial phase serving as the chondral compartment; therefore, the mechanical data reported in our study should be read as characterizing that deep load-bearing phase rather than the chondral layer alone.

Glenohumeral focal chondral defects are uncommon and frequently proceed to arthroplasty rather than a cartilage-preserving repair [3], narrowing the clinical niche. If a more clearly load-bearing indication is wanted, capitellar osteochondritis dissecans can be a more compelling one; a well-defined focal lesion in adolescent throwing athletes and gymnasts, attributed to repetitive valgus compression and shear across the radiocapitellar joint during the late cocking and acceleration phases of throwing, and to axial compression through the extended elbow during upper-extremity weight-bearing [21]. The radiocapitellar articulation carries the larger share of axial load transmitted across the elbow. Halls and Travill reported it as 57% versus 43% for the ulnotrochlear joint [22], and it was 57.8% across a range of flexion and forearm rotation angles in Smithson et al.'s study [23].

The measured apparent WCA values are broadly consistent with reported wettability of flat PLA and PCL films, with one exception. Static WCA for flat PLA films reported in previous studies is in the range of about 65–85° [24, 25]. For the PLA specimen with honeycomb architecture, the value was about 67°, which is within this range; therefore, it cannot be solely attributed to the printed architecture, but rather to the bulk polymer. PCL films have generally about 80° WCA, which is above the 56° angle measured in our study for the PCL scaffold with honeycomb architecture. This departure from the flat-film expectation is consistent with roughness amplifying an already-hydrophobic response in the opposite direction. Since PCL is intrinsically more hydrophobic than PLA (hence has a higher flat-film angle), a rough, porous surface will be expected to move its apparent angle down, toward or even below water's neutral 90° angle, rather than raising it up. Because the droplet footprint spans several pores of the printed lattice, both values should be read as apparent composite-surface wettability rather than intrinsic material wettability. Also, neither measurement was repeated on the gyroid architecture; therefore, whether the same effect holds on its more continuously curved surface or not remains untested.

The anisotropy findings in this study were based on a single rotated specimen; this is mechanically well motivated but has not yet been replicated. Flexural values beyond approximately 10% strain, which affected most gyroid and PCL-containing groups, exceed the small-deflection assumptions of standard beam theory and were reported as apparent or indicative rather than exact values. The properties reported here describe a dry, purely elastic lattice, an incomplete model of cartilage mechanics. Native cartilage carries load substantially through interstitial fluid pressurization rather than solid-phase elasticity alone, which is why the same tissue reports a Young's modulus near 1 MPa while an instantaneous modulus above 50 MPa depends on loading rate [19]. A dry lattice cannot reproduce this rate dependence, while a hydrated, hydrogel-filled lattice, which converts the construct into a biphasic system, can be used. It can be followed by filling the recommended gyroid/hybrid configuration with a GelMA-based hydrogel, ideally co-networked with methacrylated chondroitin sulfate or hyaluronic acid, and assessing time-dependent behavior via stress-relaxation and dynamic testing. Since neither PLA nor PCL bonds directly to GelMA, this will require a surface-functionalization step beforehand, such as the hyaluronic acid-based coating strategies reported for PCL scaffolds [13, 26, 27], with even infiltration through the gyroid's interior, not just its outer surface, as the main technical hurdle ahead of the biological evaluation (cytotoxicity per ISO 10993-5 [28], attachment efficiency, and general morphology) planned for the following phase.

Conclusion

This study aimed to identify a scaffold configuration suited to the mechanical and geometric limitations of the glenohumeral joint by using 3D-printed PLA/PCL osteochondral scaffolds with varying pore architecture and composition. Gyroid architecture outperformed honeycomb architecture; it reduced elastic modulus toward the native cartilage range, eliminated the pronounced off-axis weakness inherent to a strut-based lattice, and failed gradually rather than suddenly in bending; properties better matched to a joint with a small, migrating contact patch and with no fixed loading axis rather than to one loaded on a single principal direction. Composition presented a less clear-cut mechanical picture, with PCL and the layered PLA/PCL hybrid scaffolds trading off elastic modulus against plateau strength, but the hybrid's degradation profile, thermoformability to the convex humeral head, and inherently stratified structure gave it the stronger overall case as the chondral-phase material. FTIR confirmed that printing did not chemically alter the polymer, and apparent WCA were broadly consistent with reported values for the constituent materials, with roughness-related departures noted for PCL.

Therefore, a gyroid-architecture, layered PLA/PCL hybrid scaffold, PCL-rich at the articulating surface and PLA-rich in the deep load-bearing phase, is recommended as the configuration best suited to application in the glenohumeral joint. This recommendation remains provisional, since sample sizes were small, the anisotropy finding was based on a single specimen, several flexural values beyond small-deflection limits were indicative rather than exact, and wettability was not assessed on the surfaces of hybrid scaffolds or those with gyroid architecture. Moreover, the results describe a dry, purely elastic lattice, which cannot capture the fluid-pressurized, rate-dependent mechanics that define native cartilage. Therefore, it is recommended to integrate this configuration with a hydrogel matrix, characterize its time-dependent mechanical behaviors, and conduct the biological evaluation needed before the design for translational development.

Ethical Considerations

Compliance with ethical guidelines

All research ethical principles were considered in this research.

Funding

This research did not receive any grant from funding agencies in the public, commercial, or non-profit sectors.

Authors' contributions

Conceptualization and writing: Hosein Rostamani and Omid Fakhraei; Methodology: Melina Jalalian and Amirmohammad Shabanzadeh; Investigation: Melina Jalalian, Amirmohammad Shabanzadeh, Fatemeh Rahdari and Minoo Fanaei Bonakdar; Data analysis: Fatemeh Rahdari and Minoo Fanaei Bonakdar.

Conflict of interest

The authors declared no conflict of interest.

Acknowledgments

The authors would like to thank Masoud Mirzaee for his valuable assistance.

References

[1] Lara-Bertrand AL, Lizarazo-Fonseca L, Correa-Araujo L, Salguero G, Silva-Cote I. Innovative technologies for articular cartilage repair: research, development, and clinical translation, a narrative review. Journal of Functional Biomaterials. 2026; 17(3):128. [DOI:10.3390/jfb17030128] [PMID]

[2] Rostamani H, Fakhraei O, Kelidari N, Toosizadeh Khorasani F. Improving biological and mechanical properties of bioprinted PCL-alginate-chondrocyte scaffolds for patellofemoral cartilage tissue regeneration. Journal of Biomaterials Science, Polymer Edition. 2024; 35(16):2549-69. [DOI:10.1080/09205063.2024.2385182] [PMID]

[3] Seidl AJ, Kraeutler MJ. Management of articular cartilage defects in the glenohumeral joint. The Journal of The American Academy of Orthopaedic Surgeons. 2018; 26(11):e230-7. [DOI:10.5435/JAAOS-D-17-00057] [PMID]

[4] Bergmann G, Graichen F, Bender A, Kääb M, Rohlmann A, Westerhoff P. In vivo glenohumeral contact forces - measurements in the first patient 7 months postoperatively. Journal of Biomechanics. 2007; 40(10):2139-49. [DOI:10.1016/j.jbiomech.2006.10.037] [PMID]

[5] Westerhoff P, Graichen F, Bender A, Halder A, Beier A, Rohlmann A, et al. In vivo measurement of shoulder joint loads during activities of daily living. Journal of Biomechanics. 2009; 42(12):1840-9. [DOI:10.1016/j.jbiomech.2009.05.035] [PMID]

[6] Bergmann G, Graichen F, Bender A, Rohlmann A, Halder A, Beier A, et al. In vivo gleno-humeral joint loads during forward flexion and abduction. Journal of Biomechanics. 2011; 44(8):1543-52. [DOI:10.1016/j.jbiomech.2011.02.142] [PMID]

[7] Carlson CG, Chen A, Patterson K, Ablove RH. Glenohumeral cartilage thickness: implications in prosthetic design and osteochondral allograft transplantation. Cartilage. 2023; 14(3):278-84. [DOI:10.1177/19476035231154504] [PMID]

[8] Gibson LJ, Ashby MF. Cellular Solids: Structure and Properties. 2nd ed. Cambridge: Cambridge University Press; 1997. [DOI:10.1017/CBO9781139878326]

[9] Zhang B, Huang J, Narayan RJ. Gradient scaffolds for osteochondral tissue engineering and regeneration. Journal of Materials Chemistry. 2020; 8(36):8149-70. [DOI:10.1039/D0TB00688B] [PMID]

[10] Rostamani H, Firouzfar S, Fakhraei O, Nakhaei N, Shahraki N, Rafienia M. Dual-functionalized electrospun PLA/PCL blend scaffolds as bioactive platforms for osteochondral tissue engineering. International Journal of Polymeric Materials and Polymeric Biomaterials. 2026; 1-7. [DOI:10.1080/00914037.2026.2690024]

[11] Rostamani H, Fakhraei O, Paranion H, Mousazadeh Moghaddam A, Khosravi MJ. Numerical and Experimental Analysis of Geometric Patterns in FDM-printed PCL Bone Scaffolds. Journal of Translational Regenerative Medicine. 2025; 1:E1019. [Link]

[12] Woodruff MA, Hutmacher DW. The return of a forgotten polymer - polycaprolactone in the 21st century. Progress in Polymer Science. 2010; 35(10):1217-56. [DOI:10.1016/j.progpolymsci.2010.04.002]

[13] Fakhraei O, Rostamani H, Aliebrahim Nosh Abad A, Valizadeh S, Bakhshayeshi MM, Rafienia M. Enhanced biological properties of polyvinyl alcohol-polycaprolactone/hyaluronic acid-coated electrospun scaffolds for articular cartilage regeneration. Journal of Biomaterials Science, Polymer Edition. 2025; 36(15):2187-215. [DOI:10.1080/09205063.2025.2492462] [PMID]

[14] Rostamani H, Fakhraei O, Zamirinadaf N, Mahjour M. An overview of nasal cartilage bioprinting: From bench to bedside. Journal of Biomaterials Science, Polymer edition. 2024; 35(8):1273-320. [DOI:10.1080/09205063.2024.2321636] [PMID]

[15] Moayedee Y, Nikzad L, Fakhraei O, Paykar Z, Zekavat E. Improvement of mechanical, biological, and electrochemical properties of Ti6Al4V alloy modified with Nb and Ag for biomedical applications. Journal of Alloys and Compounds. 2024; 972:172736. [DOI:10.1016/j.jallcom.2023.172736]

[16] Maevskaia E, Guerrero J, Ghayor C, Bhattacharya I, Weber FE. Triply periodic minimal surface-based scaffolds for bone tissue engineering: A mechanical, in vitro and in vivo study. Tissue Engineering. Part A. 2023; 29(19-20):507-17. [DOI:10.1089/ten.tea.2023.0033] [PMID]

[17] Benya PD, Shaffer JD. Dedifferentiated chondrocytes reexpress the differentiated collagen phenotype when cultured in agarose gels. Cell. 1982; 30(1):215-24. [DOI:10.1016/0092-8674(82)90027-7] [PMID]

[18] Cao B, Peng R, Li Z, Ding J. Effects of spreading areas and aspect ratios of single cells on dedifferentiation of chondrocytes. Biomaterials. 2014; 35(25):6871-81. [DOI:10.1016/j.biomaterials.2014.04.107] [PMID]

[19] Kabir W, Di Bella C, Choong PFM, O'Connell CD. Assessment of native human articular cartilage: A biomechanical protocol. Cartilage. 2021; 13(2_suppl):427S-37S. [DOI:10.1177/1947603520973240] [PMID]

[20] Soslowsky LJ, Flatow EL, Bigliani LU, Mow VC. Articular geometry of the glenohumeral joint. Clinical Orthopaedics & Related Research. 1992; 285:181-90. [DOI:10.1097/00003086-199212000-00023]

[21] Kajiyama S, Muroi S, Sugaya H, Takahashi N, Matsuki K, Kawai N, et al. Osteochondritis dissecans of the humeral capitellum in young athletes: Comparison Between Baseball Players and Gymnasts. Orthopaedic Journal of Sports Medicine. 2017; 5(3):2325967117692513. [DOI:10.1177/2325967117692513] [PMID]

[22] Halls AA, Travill A. Transmission of pressures across the elbow joint. The Anatomical Record. 1964; 150:243-7. [DOI:10.1002/ar.1091500305] [PMID]

[23] Smithson K, Smith J, Hogue W, Mannen E, Ahmadi S. Biomechanics of axial load transmission across the native human elbow. Shoulder & Elbow. 2021; 13(6):671-6. [DOI:10.1177/1758573220961025] [PMID]

[24] Tümer EH, Erbil HY, Akdoğan N. Wetting of superhydrophobic polylactic acid micropillared patterns. Langmuir. 2022; 38(32):10052-64. [DOI:10.1021/acs.langmuir.2c01708] [PMID]

[25] Luque-Agudo V, Gallardo-Moreno AM, González-Martín ML. Influence of solvent and substrate on hydrophobicity of PLA films. Polymers. 2021; 13(24):4289. [DOI:10.3390/polym13244289] [PMID]

[26] Sohrabi M, Hesaraki S, Shahrezaee M, Shams-Khorasani A. The release behavior and in vitro osteogenesis of quercetin-loaded bioactive glass/hyaluronic acid/sodium alginate nanocomposite paste. International Journal of Biological Macromolecules. 2024; 280(Pt 4):136094. [DOI:10.1016/j.ijbiomac.2024.136094] [PMID]

[27] Komaei FM, Hesaraki S, Akbari G, Jahandideh A. Infected bone defect healing could be complicated due to more delayed responses to antibiotic therapy in ovariohysterectomized rats. Archives of Veterinary Science. 2025; 30(1):1. [DOI:10.5380/avs.v30i1.96162]

[28] International Organization for Standardization. ISO 10993-5:2009. Biological evaluation of medical devices, Part 5: Tests for in vitro cytotoxicity. Vernie: International Organization for Standardization: 2009. [Link]